Multifrequency study of SNR J0533–7202, a new supernova remnant in the LMC

L. M. Bozzetto,[1] M. D. Filipović,[1] E.J. Crawford,[1] M. Sasaki,[2] P. Maggi,[3] F. Haberl,[3] D. Urošević,[4,5] J. L. Payne,[1] A. Y. De Horta,[1] M. Stupar,[6,7] R. Gruendl,[8] & J. Dickel[9]

[1] *School of Computing and Mathematics, University of Western Sydney Locked Bag 1797, Penrith South DC, NSW 1797, Australia*
[2] *Institut für Astronomie und Astrophysik Tübingen, Sand 1, D-72076 Tübingen, Germany*
[3] *Max-Planck-Institut für extraterrestrische Physik, Giessenbachstraße, D-85748 Garching, Germany*
[4] *Department of Astronomy, Faculty of Mathematics, University of Belgrade, Studentski trg 16, 11000 Belgrade, Serbia*
[5] *Isaac Newton Institute of Chile, Yugoslavia Branch*
[6] *Department of Physics, Macquarie University, Sydney, NSW 2109, Australia*
[7] *Australian Astronomical Observatory, PO Box 296, Epping, NSW 1710, Australia*
[8] *Department of Astronomy, University of Illinois, 1002 West Green Street, Urbana, IL 61801, USA*
[9] *Physics and Astronomy Department, University of New Mexico, MSC 07-4220, Albuquerque, NM 87131, USA*

ABSTRACT

We present a detailed study of Australia Telescope Compact Array (ATCA) observations of a newly discovered Large Magellanic Cloud (LMC) supernova remnant (SNR), SNR J0533–7202. This object follows a horseshoe morphology, with a size 37 pc × 28 pc (1-pc uncertainty in each direction). It exhibits a radio spectrum with the intrinsic synchrotron spectral index of α=–0.47±0.06 between 73 and 6 cm. We report detections of regions showing moderately high fractional polarisation at 6 cm, with a peak value of 36±6% and a mean fractional polarisation of 12±7%. We also estimate an average rotation measure across the remnant of –591 rad m^{-2}. The current lack of deep X-ray observation precludes any conclusion about high-energy emission from the remnant. The association with an old stellar population favours a thermonuclear supernova origin of the remnant.

Key words: supernova remnants – Large Magellanic Cloud – SNR 0533-7202.

1 INTRODUCTION

Supernova remnants (SNRs) are responsible for the distribution of heavy elements in the universe, influencing the chemical composition of the next generation of stars. SNRs have a significant effect on their environment, heating up the surrounding gas and dust as the shock waves of the supernova explosion pass through. In turn however, SNRs are heavily impacted by their environment, as their evolution, structure and expansion is greatly affected by the density of the surrounding ISM. In the radio-continuum, SNR emission is predominately non-thermal and will typically display a radio spectral index of $\alpha \sim$ –0.5 (defined by $S \propto \nu^{\alpha}$). However, this may significantly vary due to environmental factors, different stages of evolution and various types of SNRs.

The Large Magellanic Cloud (LMC) is an irregular dwarf galaxy in close proximity to our own Milky Way galaxy at a distance of 50 kpc (Macri et al. 2006). As a re-

sult of this relatively close distance, objects in the LMC can be observed with significantly better spatial resolution and sensitivity than those in other galaxies. However, it is far away enough that we are able to assume all objects that lie within the galaxy are at very similar distances, therefore making estimates for various analysis methodologies such as extent and surface brightness more accurate, as these values depend on accurate distances to the object. In contrast, objects in the Milky Way can be hard to find accurate distances for, and therefore leads to imprecise measurements. The LMC is also a desirable environment for various astronomical studies as it contains some of the most active star forming regions in our Local Group of galaxies as well as residing outside of the Galactic plane, at a moderate inclination angle of 35° (van der Marel & Cioni 2001), which greatly minimises the interference from stars, gas, and dust within the LMC.

In this paper, we report on a newly discovered LMC SNR, SNR J0533–7202. Radio observations of this object

were also taken by Filipovic et al. (1995, 1998a,b) in their surveys of the Magellanic Clouds, however, they did not classify this object. The new observations, data reduction and imaging techniques are described in Section 2. The astrophysical interpretation of newly obtained moderate-resolution total intensity and polarimetric images in combination with the existing Magellanic Cloud Emission Line Survey (MCELS) images are discussed in Section 3.

2   OBSERVATIONS AND DATA REDUCTION

We observed SNR J0533–7202 with the ATCA on the 15th and 16th of November 2011, using the new Compact Array Broadband Backend (CABB) at array configuration EW367 and at wavelengths of 3 and 6 cm (ν=9000 and 5500 MHz). Baselines formed with the 6th ATCA antenna were excluded, as the other five antennas were arranged in a compact configuration. The observations were carried out in the so called "snap-shot" mode, totaling ∼50 minutes of integration over a 14 hour period. PKS B1934-638 was used for flux density calibration[1] and PKS B0530-727 was used for secondary (phase) calibration. The phase calibrator was observed twice every hour for a total 78 minutes over the whole observing session. The MIRIAD[2] (Sault et al. 1995) and KARMA (Gooch 1995) software packages were used for reduction and analysis. More information on the observing procedure and other sources observed in this project can be found in Bozzetto et al. (2012a,b) and de Horta et al. (2012).

The CABB 2 GHz bandwidth is a 16 times improvement from the previous 128 MHz, and with the new higher data sampling has increased the sensitivity of the ATCA by a factor of 4. The 2 GHz bandwidth not only aids in high sensitivity observations, but also allows data to be split into channels which can then be used for measuring Faraday rotation across the entire bandwidth, at frequencies close enough that the $n \times 180°$ ambiguities prevalent when making an estimate between distant frequencies, are no longer an issue.

Images were formed using MIRIAD multi-frequency synthesis (Sault & Wieringa 1994) and natural weighting. They were deconvolved with primary beam correction applied. The same procedure was used for both U and Q stokes parameter maps.

The 3 cm image (Fig. 1) has a resolution (full width half maximum (FWHM)) of $21.6'' \times 15.0''$ (PA=47.2°). Similarly, we made an image of SNR J0533–7202 at 6 cm (seen as contours in Fig. 1) which has a FWHM of $34.1'' \times 26.1''$ at PA=45.5° and an estimated r.m.s. noise of 0.3 mJy/beam.

3   RESULTS AND DISCUSSION

This new LMC remnant exhibits a horseshoe morphology (Fig. 1), centered at RA(J2000)=$5^h 33^m 46.5^s$, DEC(J2000)=$-72°02'59''$. We selected a one-dimensional intensity profile across the approximate major (NW–SE) and minor (NE–SW) axis (PA=45°) (Fig. 2) at the 3σ noise level (0.9 mJy) to estimate the spatial extent of SNR J0533–7202.

Its size at 6 cm is $152'' \times 115''$ with a $4''$ uncertainty in each direction (37×28 pc with a 1 pc uncertainty in each direction). We did not detect any [O III] or [S II] emission in the Magellanic Cloud Emission Line Survey (MCELS) (Smith et al. 2006) images. However, there is some tentative and very faint Hα emission possibly associated with this SNR which wasn't evident anywhere else in the field surrounding the remnant. Although, more sensitive observations are needed.

An X-ray source at the rim of the SNR was detected in the course of the ROSAT all-sky survey and was given the identifier 1RXS J053353.6-720404 (Voges et al. 1999). However, the likelihood of existence[3] in these observations was only 7, meaning only a 3.3σ detection, and therefore not much could be done with respect to the X-ray analysis, apart from plotting the ROSAT position (Fig. 1). This ROSAT position is slightly south-west of one of the radio-bright regions of the remnant. Low statistics preclude any classification between an extended or compact source.

This SNR did not appear in the Spitzer mosaic images of the LMC (Meixner et al. 2006), neither at the 3.6, 4.5, 5.8, and 8 μm wavelengths of the IRAC instrument (Fazio et al. 2004), nor in the 24, 70, and 160 μm bands of the MIPS instrument (Rieke et al. 2004), suggesting that there is no association with mid or near-infrared wavelengths. There are no OB star candidates in the Magellanic Clouds Photometric Survey (MCPS) catalogue (Zaritsky et al. 2004) within a 100 pc radius around the centre of the remnant, and the star formation history map of the LMC (Harris & Zaritsky 2009) shows no recent episode of star formation activity in the neighbourhood. The association of SNR J0533-7202 with an old stellar population favours a thermonuclear supernova origin of the remnant.

We based the spectral energy distribution (SED) on our own integrated flux estimates, coupled with the 73 cm measurement by Clarke et al. (1976). These values are shown in Table 1 and then used to produce a spectral index graph (Fig. 3). The point source (ATCA J0534–7201; see Fig. 1) to the east of SNR J0533–7202 was unresolved from the SNR in the 73 cm survey (MC4; Clarke et al. 1976). We estimate 36 cm flux density measurements from the Molonglo Synthesis Telescope (MOST) mosaic image (as described in Mills et al. 1984) and a 36 cm SUMMS mosaic image (Mauch et al. 2008). We point that these values differ some 25%, which is most likely due to the higher sensitivity of the MOST image and its greater UV coverage. The 20 cm flux density was measured from a mosaic image published by Hughes et al. (2007). Two different sets of images were used to estimate integrated flux densities at wavelengths of 6 & 3 cm. The first set (5500 & 9000 MHz) contains our CABB observations merged with the mosaic visibility files from Dickel et al. (2005). These observations use the EW 367 array, which has a shortest baseline of 46 m and as a result, has missing flux from the lack of short spacings. The second set of images (4800 & 8640 MHz) are from the mosaic images published by Dickel et al. (2010), which used EW 367 and EW 352 arrays at both frequencies as well as Parkes at 4800 MHz but not at 8640 MHz, as the Parkes

---

[3] In the ROSAT source detection a likelihood L is associated to a probability of a detected source being real P by P = 1 - exp(-L).

survey at 3 cm did not extend that far south. This survey data had more spatial frequency coverage, particularly for the extended emission, but less sensitivity. We can see the detrimental effect of missing short spacings in the 3 cm flux density measurements, where they fall well below the trend of the SED at higher wavelengths (Fig. 3). Due to the significant impact of the missing shorter spacings (and as a result, missing flux), we omit the 3 cm measurements from the calculation, leaving all the frequencies up to 6 cm (5500 MHz), and thus a spectral index of α=–0.47±0.06.

Fractional polarisation (P) was calculated at 6 cm using:

$$P = \frac{\sqrt{S_Q^2 + S_U^2}}{S_I} \qquad (1)$$

where S_Q, S_U and S_I are integrated intensities for Q, U and I Stokes parameters (Fig. 4). Our estimated peak value is 36±6% with a mean fractional polarisation of 12±7%. This level of fractional polarisation is relatively high when compared to various other SNRs in the LMC (Cajko et al. 2009; Crawford et al. 2010; Bozzetto et al. 2012a) and would be (theoretically) expected for an SNR with a radio spectrum of around or less than –0.5 (Rolfs & Wilson 2003). This may indicate varied dynamics along the shell.

Polarisation position angles were taken from across the 2 GHz bandwidth (at 5500 MHz split into 128 MHz channels) and used to estimate the Faraday rotation for this SNR. The result of this can be seen in Fig. 5, with the open boxes representing negative values of rotation measure and the filled in boxes representing positive rotation measure. The rotation measure varies quite significantly along the SNR with the most change being negative rotation measure near the peak intensity in the western region of the remnant. The average rotation measure across the SNR was –591 rad m^{-2}. This value is nearly double that of the plerion in SNR G326.3–1.8 (Dickel et al. 2000) and significantly exceeds what is typical of 'large' values in the LMC and Milky Way of ±250 rad m^{-2} (Dickel & Milne 1995). It would be best to treat this value with some level of caution, as at higher radio frequencies – such as our 6 cm observations – the amount of rotation measure expected from a SNR is within the same range as the expected error. To mitigate this error and achieve a more reliable value of rotation measure, additional observations would need to be taken, preferably at lower radio frequencies where we would expect a higher level of rotation measure.

We were also able to estimate the magnetic field strength for this SNR based on the equipartition formula as given in Arbutina et al. (2012). This formula is based on the Bell (1978) diffuse shock acceleration (DSA) theory. By using the spectral index value α=–0.5, we get an equipartition value for SNR J0533–7202 of ∼45 μG with an estimated minimum energy of $E_{min} = 9.4 \times 10^{49}$ ergs.

From the position of SNR J0533–7202 at the surface brightness to diameter (Σ - D) diagram ((D, Σ) = (32.5 pc, 6.2×10^{-21} W m^{-2} Hz^{-1} sr^{-1})) by Berezhko & Völk (2004), we can estimate that SNR J0533–7202 is likely to be an SNR in the late energy conserving phase, with an explosion energy between 0.25 and 1×10^{51} ergs, which evolves in an environment of density ∼1 cm^{-3}.

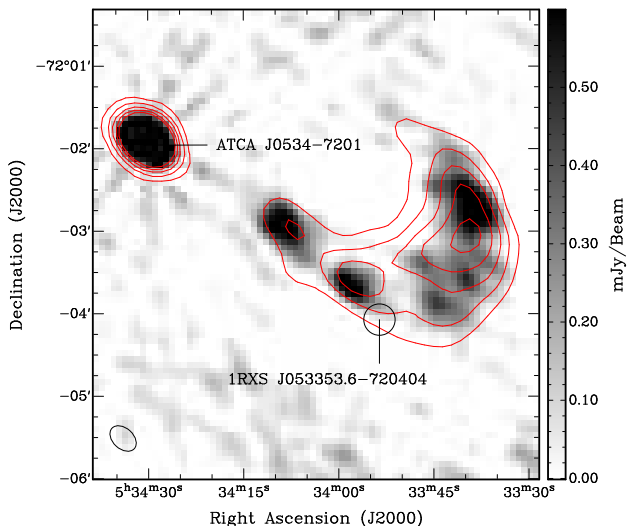**Figure 1.** ATCA observations of SNR J0533–7202 at 3 cm (9000 MHz) overlaid with 6 cm (5500 MHz) contours. The contours are 3, 6, 9, 12 & 15σ. The ellipse in the lower left corner represents the synthesised beamwidth (at 6 cm) of 34.1″×26.1″. The sidebar quantifies the pixel map. The overlaid circle shows the position of a weak X-ray source seen by ROSAT.

4 CONCLUSION

We have added a new SNR to the LMC SNR population through conducting a high resolution radio–continuum study of SNR J0533–7202. We report a relatively large SNR with an extent of ∼152″×115″ (∼37×28 pc), and a radio spectral index with α=–0.47 between 73 and 6 cm. We estimate fractional polarisation of the remnant at 6 cm with a peak of 36±6% and a mean integrated value of 12±7%. The lack of recent star formation activity around the remnant makes a thermonuclear supernova origin more likely.

REFERENCES

Arbutina B., Urošević D., Andjelić M. M., Pavlović M. Z., Vukotić B., 2012, ApJ, 746, 79
Bell A. R., 1978, MNRAS, 182, 443
Berezhko E. G., Völk H. J., 2004, A&A, 427, 525
Bozzetto L. M., Filipović M. D., Crawford E. J., Haberl F., Sasaki M., Urošević D., Pietsch W., Payne J. L., de Horta

Table 1. Integrated flux densities of SNR J0533–7202 and the point source ATCA J0534–7201.

ν (MHz)	λ (cm)	R.M.S (mJy)	Beam Size ($''$)	S_{PS} (mJy)	ΔS_{PS} (mJy)	S_{SNR} (mJy)	ΔS_{SNR} (mJy)	Reference
73	408	40	157.2×171.6	—	—	220	22	Clarke et al. (1976)
36[a]	843	0.8	46.4×43.0	34	3	153	15	This work
36[b]	843	1.0	46.4×43.0	39	4	117	12	This work
20	1384	0.6	40.0×40.0	31	3	120	12	This work
6	4800	0.7	35.0×35.0	24	2	72	7	This work
6	5500	0.3	34.1×26.1	20	2	54	5	This work
3[c]	8640	0.7	22.0×22.0	19	2	23	2	This work
3[c]	9000	0.3	21.6×15.0	17	2	22	2	This work

[a] – Uses the MOST mosaic image
[b] – Uses the SUMMS mosaic image
[c] – Due to short spacing, these 3 cm flux density estimates are omitted from the SNR SED estimate.

A. Y., Stupar M., Tothill N. F. H., Dickel J., Chu Y.-H., Gruendl R., 2012a, MNRAS, 420, 2588

Bozzetto L. M., Filipovic M. D., Crawford E. J., Payne J. L., de Horta A. Y., Stupar M., 2012b, Rev. Mexicana Astron. Astrofis., 48, 41

Cajko K. O., Crawford E. J., Filipovic M. D., 2009, Serbian Astronomical Journal, 179, 55

Clarke J. N., Little A. G., Mills B. Y., 1976, Australian Journal of Physics Astrophysical Supplement, 40, 1

Crawford E. J., Filipović M. D., Haberl F., Pietsch W., Payne J. L., de Horta A. Y., 2010, A&A, 518, A35

de Horta A. Y., Filipović M. D., Bozzetto L. M., Maggi P., Haberl F., Crawford E. J., Sasaki M., Urošević D., Pietsch W., Gruendl R., Dickel J., Tothill N. F. H., Chu Y.-H., Payne J. L., Collier J. D., 2012, A&A, 540, A25

Dickel J. R., McIntyre V. J., Gruendl R. A., Milne D. K., 2005, AJ, 129, 790

Dickel J. R., Milne D. K., 1995, AJ, 109, 200

Dickel J. R., Milne D. K., Strom R. G., 2000, ApJ, 543, 840

Fazio G. G., Hora J. L., Allen L. E., Ashby M. L. N., Barmby P., Deutsch L. K., Huang J.-S., Kleiner S., Marengo M., Megeath S. T., Melnick G. J., Pahre M. A., Patten B. M., Polizotti J., Smith H. A., Taylor R. S., Wang Z., Willner S. P., Hoffmann W. F., Pipher J. L., Forrest W. J., McMurty C. W., McCreight C. R., McKelvey M. E., McMurray R. E., Koch D. G., Moseley S. H., Arendt R. G., Mentzell J. E., Marx C. T., Losch P., Mayman P., Eichhorn W., Krebs D., Jhabvala M., Gezari D. Y., Fixsen D. J., Flores J., Shakoorzadeh K., Jungo R., Hakun C., Workman L., Karpati G., Kichak R., Whitley R., Mann S., Tollestrup E. V., Eisenhardt P., Stern D., Gorjian V., Bhattacharya B., Carey S., Nelson B. O., Glaccum W. J., Lacy M., Lowrance P. J., Laine S., Reach W. T., Stauffer J. A., Surace J. A., Wilson G., Wright E. L., Hoffman A., Domingo G., Cohen M., 2004, ApJS, 154, 10

Filipovic M. D., Haynes R. F., White G. L., Jones P. A., 1998a, A&AS, 130, 421

Filipovic M. D., Haynes R. F., White G. L., Jones P. A., Klein U., Wielebinski R., 1995, A&AS, 111, 311

Filipovic M. D., Pietsch W., Haynes R. F., White G. L., Jones P. A., Wielebinski R., Klein U., Dennerl K., Ka-

habka P., Lazendic J. S., 1998b, A&AS, 127, 119

Gooch R., 1995, in Shaw R. A., Payne H. E., Hayes J. J. E., eds, Astronomical Data Analysis Software and Systems IV Vol. 77 of Astronomical Society of the Pacific Conference Series, Space and the Spaceball. p. 144

Harris J., Zaritsky D., 2009, AJ, 138, 1243

Hughes A., Staveley-Smith L., Kim S., Wolleben M., Filipović M., 2007, MNRAS, 382, 543

Macri L. M., Stanek K. Z., Bersier D., Greenhill L. J., Reid M. J., 2006, ApJ, 652, 1133

Mauch T., Murphy T., Buttery H. J., Curran J., Hunstead R. W., Piestrzynski B., Ropbertson J. G., Sadler E. M., 2008, VizieR Online Data Catalog, 8081, 0

Meixner M., Gordon K. D., Indebetouw R., Hora J. L., Whitney B., Blum R., Reach W., Bernard J.-P., Meade M., Babler B., Engelbracht C. W., For B.-Q., Misselt K., Vijh U., Leitherer C., Cohen M., Churchwell E. B., Boulanger F., Frogel J. A., Fukui Y., Gallagher J., Gorjian V., Harris J., Kelly D., Kawamura A., Kim S., Latter W. B., Madden S., Markwick-Kemper C., Mizuno A., Mizuno N., Mould J., Nota A., Oey M. S., Olsen K., Onishi T., Paladini R., Panagia N., Perez-Gonzalez P., Shibai H., Sato S., Smith L., Staveley-Smith L., Tielens A. G. G. M., Ueta T., van Dyk S., Volk K., Werner M., Zaritsky D., 2006, AJ, 132, 2268

Mills B. Y., Turtle A. J., Little A. G., Durdin J. M., 1984, Australian Journal of Physics, 37, 321

Rieke G. H., Young E. T., Engelbracht C. W., Kelly D. M., Low F. J., Haller E. E., Beeman J. W., Gordon K. D., Stansberry J. A., Misselt K. A., Cadien J., Morrison J. E., Rivlis G., Latter W. B., Noriega-Crespo A., Padgett D. L., Stapelfeldt K. R., Hines D. C., Egami E., Muzerolle J., Alonso-Herrero A., Blaylock M., Dole H., Hinz J. L., Le Floc'h E., Papovich C., Pérez-González P. G., Smith P. S., Su K. Y. L., Bennett L., Frayer D. T., Henderson D., Lu N., Masci F., Pesenson M., Rebull L., Rho J., Keene J., Stolovy S., Wachter S., Wheaton W., Werner M. W., Richards P. L., 2004, ApJS, 154, 25

Rolfs K., Wilson T., 2003, Tools of Radio Astronomy 4ed. Springer

Sault R. J., Teuben P. J., Wright M. C. H., 1995, in Shaw R. A., Payne H. E., Hayes J. J. E., eds, Astronomical Data Analysis Software and Systems IV Vol. 77 of Astronomical
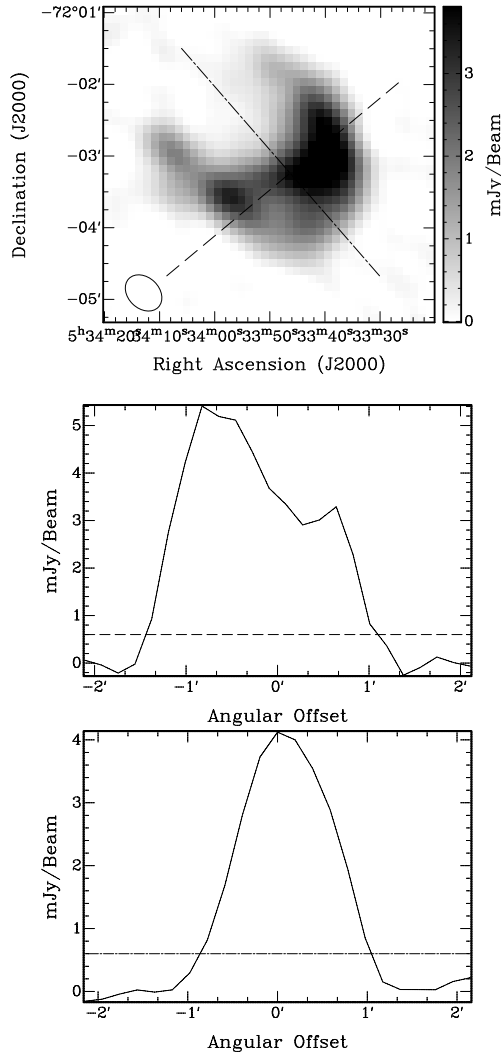
Figure 2. The top image shows the 6 cm intensity image of overlaid with the approximate major (NW–SE) and minor (NE–SW) axis. The middle and lower images show the 1-dimensional cross-section along the overlaid lines in the top image, with a superimposed line at 3σ.

Society of the Pacific Conference Series, A Retrospective View of MIRIAD. p. 433

Sault R. J., Wieringa M. H., 1994, A&AS, 108, 585

Smith C., Points S., Winkler P. F., 2006, NOAO Newsletter, 85, 6

van der Marel R. P., Cioni M.-R. L., 2001, AJ, 122, 1807

Voges W., Aschenbach B., Boller T., Bräuninger H., Briel U., Burkert W., Dennerl K., Englhauser J., Gruber R., Haberl F., Hartner G., Hasinger G., Kürster M., Pfeffermann E., Pietsch W., Predehl P., Rosso C., Schmitt J. H. M. M., Trümper J., Zimmermann H. U., 1999, A&A, 349, 389

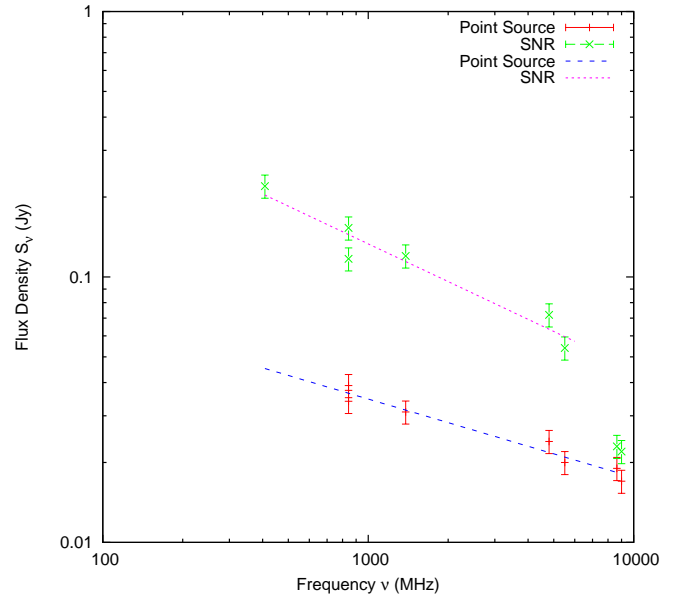Zaritsky D., Harris J., Thompson I. B., Grebel E. K., 2004, AJ, 128, 1606

Figure 3. Radio-continuum spectrum of SNR J0533–7202 and the point source ATCA J0534–7201. The pink dotted line represents the spectral index of the SNR and the blue dashed line represents the spectrum of the point source.
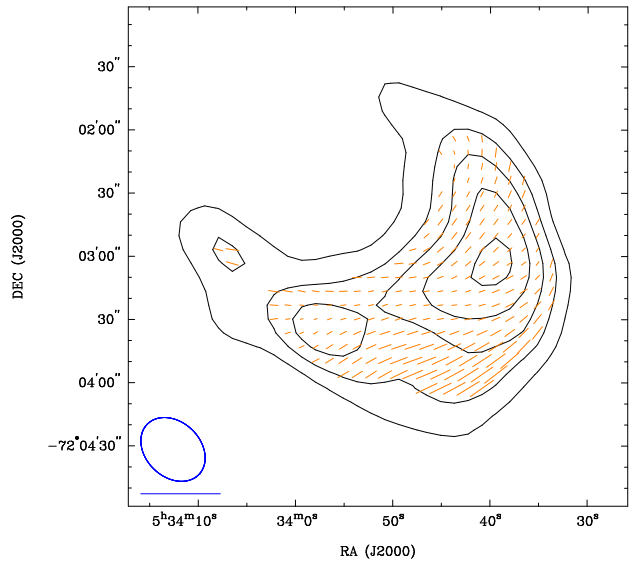

Figure 4. B–field vectors overlaid on 6 cm contours (3, 6, 9, 12 and 15σ) of SNR J0533–7202 from ATCA observations. The ellipse in the lower left corner represents the synthesised beamwidth of $34.3'' \times 26.0''$ and the line below the ellipse shows a polarisation vector of 100%.
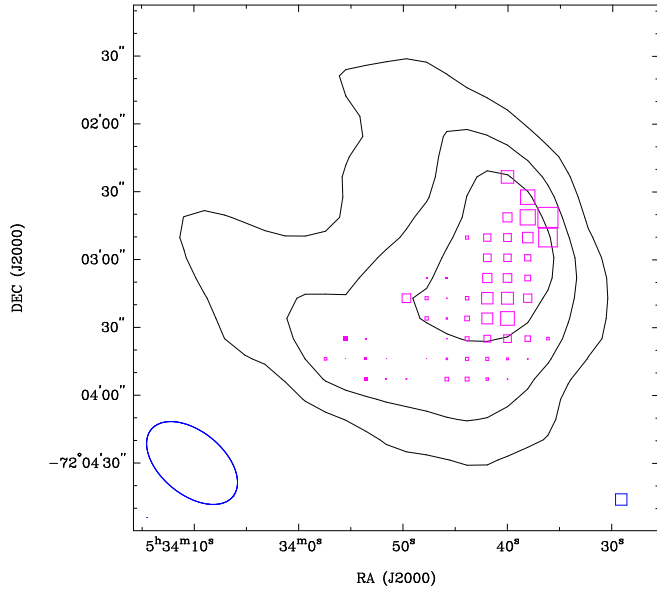
Figure 5. Faraday rotation measure of SNR J0533–7202 overlaid on 6 cm (128 MHz bandwidth) ATCA contours (3, 8 & 13σ). Filled squares represent positive rotation measure while open squares represent negative rotation measure. The ellipse in the lower left corner represents the synthesised beamwidth of $46.7'' \times 27.9''$ and the box in the lower right represents a rotation measure of 1000 rad/m^2. The width of the boxes scale with rotation measure.